NEOPLASIA
www.neoplasia.com

Volume 35 Number xxx Month 2023 pp. 100847

Bacterial translocation and barrier dysfunction enhance colonic tumorigenesis ☆,☆☆,★

Yongguo Zhang [a]; Jilei Zhang [a]; Yinglin Xia [a]; Jun Sun [a,b,c,d,*]

[a] Department of Medicine, College of Medicine, University of Illinois Chicago, Chicago, IL, USA
[b] UIC Cancer Center, University of Illinois Chicago, Chicago, IL, USA
[c] Department of Microbiology/Immunology, College of Medicine, University of Illinois Chicago, Chicago, IL, USA
[d] Jesse Brown VA Medical Center Chicago, IL (537), USA

Abstract

In the development of colon cancer, the intestinal dysbiosis and disruption of barrier function are common manifestations. In the current study, we hypothesized that host factors, e.g., vitamin D receptor deficiency or adenomatous polyposis coli (APC) mutation, contribute to the enhanced dysbiosis and disrupted barrier in the pathogenesis of colorectal cancer (CRC). Using the human CRC database, we found enhanced tumor-invading bacteria and reduced colonic VDR expression, which was correlated with a reduction of Claudin-10 mRNA and protein. In the colon of $VDR^{\Delta IEC}$ mice, deletion of intestinal epithelial VDR led to lower protein of tight junction protein Claudin-10. Lacking VDR and a reduction of Claudin-10 are associated with an increased number of tumors in the mice without myeloid VDR. Intestinal permeability was significantly increased in the mice with myeloid VDR conditional deletion. Further, mice with conditional colonic APC mutation showed reduced mucus layer, enhanced bacteria in tumors, and loss of Claudin-10. Our data from human samples and colon cancer models provided solid evidence- on the host factor regulation of bacterial translocation and dysfunction on barriers in colonic tumorigenesis. Studies on the host factor regulation of microbiome and barriers could be potentially applied to risk assessment, early detection, and prevention of colon cancer.

Neoplasia (2023) 35, 100847

Keywords: Adenomatous polyposis coli (APC), Claudin, Barrier function, Inflammation, Colon cancer, Myeloid cells, Microbiome, Mucin, Tight junction, Vitamin D, Vitamin D receptor

Introduction

In the healthy colon, several barrier layers, including the balanced microbiota, strong mucus layer, epithelial barriers, and local immunity, protect the intestine against inflammation and cancer. However, the tumor development in the colon is related to the microbial dysbiosis, narrowed mucus layer, and damaged barrier functions. Moreover, these dysfunctional changes could further induce the dislocation of intestinal microbiome from the lumen to the intestinal epithelium and tumors.

Multiple factors (e.g., risk genes, environmental triggers/lifestyle, immunity, and microbiome) contribute to the pathogenesis of colorectal cancer (CRC) [1–6]. The intestinal dysbiosis and disruption of barrier function are common manifestations of CRC. Tight junction (TJ) structures are essential in intestinal innate immunity and barrier functions. Changes in expression and distribution of TJ proteins, such as Claudin -2, -5, and -8 lead to discontinuous TJs and barrier dysfunction in active Crohn's disease [7,8]. Vitamin D/Vitamin D receptor (VDR) is known to protect against dysbiosis and tumorigenesis [9]. Vitamin D is an environmental factor related to exposure to sunlight, dietary, and lifestyle, whereas VDR acts as a host factor in maintaining healthy innate immunity. Considering the multiple functional roles of VDR in the development of cancer, it is important to

* Corresponding author.
E-mail address: junsun7@uic.edu (J. Sun).

☆ Author Contributions: YZ: acquisition, analysis, and interpretation of data; drafting the figures and manuscript; and statistical analysis. JZ: assistance with animal models, western blots, and figure drafting. YX: statistical analysis, and manuscript drafting. JS: study concept and design, analysis and interpretation of data, writing the manuscript for important intellectual content, obtained funding, and study supervision.

☆☆ Funding: This research was funded by the UIC Cancer Center, the NIDDK/National Institutes of Health grant R01 DK105118 and R01DK114126, VA Merit Award VA 1 I01 BX004824-01, and DOD BC160450P1 to Jun Sun**.** The study sponsors played no role in the study design, data collection, analysis, and interpretation of data. The contents do not represent the views of the United States Department of Veterans Affairs or the United States Government.

★ Conflicts of Interest: The authors declare no conflict of interest. The funders played no role in the study design, the collection, analyses, or interpretation of data, the writing of the manuscript, or the decision to publish the results.

Received 3 August 2022; received in revised form 17 October 2022; accepted 19 October 2022

https://doi.org/10.1016/j.neo.2022.100847

dissect the mechanisms by which VDR contributes to barrier function in protecting the host from tumorigenesis.

In the current study, we tested the hypothesis that a host factor, e.g., VDR deficiency or adenomatous polyposis coli (APC) mutation [10], leads to the reduced thickness of mucus layer and enhanced penetration of microbiota into the epithelial cells, thus enhancing colonic tumorigenesis *in vivo*. The positively correlated status of VDR and Claudins (e.g., Claudin-10) contribute to the altered intestinal permeability in tumorigenesis. In the intestinal epithelial VDR knockout ($VDR^{\Delta IEC}$) mice, myeloid cell VDR deletion (VDR^{lyz}) mice, and an APC colonic mutated mouse model, bacterial translocation and inflammation in the genetic deficient context further altered TJ proteins, e.g., Claudin-10, and manipulated the barrier functions in the development of colon cancer. Studies on the host factor regulation of intestinal microbiome and barriers could be potentially applied to risk assessment, early detection, and prevention of colon cancer. These studies will provide an additional avenue to restore microbiome and barrier functions for risk assessment and prevention of CRC.

Materials and methods

Human tissue samples

This study was performed in accordance with approval from the UIC Ethics Committee (Institutional Review Board: 2017-0384). Colorectal tissue samples were obtained from 10 CRC patients with neoplasia and 10 patients without neoplasia (49–74 years old).

Gene expression datasets

For expression analyses, we used microarray data reported in the NCBI Gene Expression Omnibus database [11]. We gathered data by searching the Gene Expression Omnibus [11] (https://www.ncbi.nlm.nih.gov/geo/) for expression profiling studies using colonic biopsy samples from normal controls as well as colon cancer biopsy samples from colon cancer subjects. We randomly selected the GEO database reference GSE 21510 [12], 44 normal controls and 104 colon cancer patients were analyzed. Both were subjected to further analyses.

Animals

$VDR^{\Delta IEC}$ mice were obtained by crossing the VDR^{Loxp} mice, originally provided by Dr. Geert Carmeliet [13] with villin-cre mice (Jackson Laboratory, 004586), as we previously reported [14–16]. We further backcrossed this strain with C57BL/6 mice for more than 10 generations after arriving our animal facility [17]. $VDR^{\Delta lyz}$ mice were obtained by crossing the VDR^{LoxP} mice with Lyz-cre mice (Jackson Laboratory, 004781). $VDR^{\Delta IEC}$ mice were obtained by crossing the VDR^{Loxp} mice with villin-cre mice (Jackson Laboratory, 004586), as we previously reported [14,16]. Experiments were performed on 2-3 months old mice including male and female.

Intestinal-specific VDR-overexpressing (O-VDR) mice were generated in C57BL/6 mice strain background, as reported in our recent study [18]. VDR expression in O-VDR mice is Cre driven [18]. This O-VDR^{loxp} mouse line is labeled as O-VDR^{loxp} in our gain of function study, distinct from the $VDR^{loxP/loxP}$ mouse made for $VDR^{\Delta IEC}$ mice. Experiments were performed on 2–3 months old mice, including male and female.

The colon-specific APC knockout ($APC^{\Delta CEC}$) mice were generated by breeding APC^{15loxp} mice (Jackson Laboratory, 029275) and CDX2P-NLS Cre mice (Jackson Laboratory, 009350). The 6-8 week-old female and male APC^{15loxp} and $APC^{\Delta CEC}$ mice were randomly chosen for experimental groups. $APC^{15\Delta CEC}$ mice spontaneously developed colonic tumors at >21-week old at the UIC animal facility.

Mice were provided with water ad libitum and maintained in a 12 h dark/light cycle. The animal work was approved by the UIC Office of Animal Care. The animal work was approved by the UIC Office of Animal Care (ACC 15-231,17-218, 20-201, 21-120, and 21-177).

Induction of colon cancer by AOM-DSS in mice

Mice were treated with 10mg/kg of AOM (Sigma-Aldrich, Milwaukee, WI, USA) by intraperitoneal injection as previously described [9,19,20]. After a 7-day recovery period, mice received three cycles of 2% DSS in the drinking water. Tumor counts and measurements were performed in a blinded fashion under a stereo-dissecting microscope (Nikon SMZ1000, Melville, NY, USA). Microscopic analysis was performed for the severity of inflammation and dysplasia on hematoxylin and eosin-stained 'Swiss rolled' colons by a gastrointestinal pathologist blinded to treatment conditions.

Western blot analysis and antibodies

Mouse colonic epithelial cells were collected by scraping the tissue from the colon of the mouse, including the proximal and distal regions. The cells were sonicated in lysis buffer (10 mM Tris, pH 7.4, 150 mM NaCl, 1 mM EDTA, 1 mM EGTA, pH 8.0, 1% Triton X-100) with 0.2 mM sodium ortho-vanadate, and protease inhibitor cocktail. The protein concentration was measured using the BioRad Reagent (BioRad, Hercules, CA, USA). Equal amounts of protein were separated by SDS-polyacrylamide gel electrophoresis, transferred to nitrocellulose, and immunoblotted with primary antibodies. Villin was used as an internal control for intestinal epithelial cells. Beta-actin was also used as a control for equal loading of proteins. The following antibodies were used: anti-Claudin-10 (Invitrogen, 38-8400, Carlsbad, CA, USA), anti-Claudin-7 (Invitrogen, 34-9100, Carlsbad, CA, USA), anti-Claudin-3 (Invitrogen, 34-1700, Carlsbad, CA, USA), anti-Claudin-4 (Invitrogen, 36-4800, Carlsbad, CA, USA), anti-Claudin-7 (Invitrogen, 34-9100, Carlsbad, CA, USA), anti-villin (Santa Cruz Biotechnology, SC-58897, Dallas, TX, USA) or anti-β-actin (Sigma-Aldrich, A5316, St. Louis, MO, USA) antibodies and were visualized by ECL (Thermo Fisher Scientific, 32106, Waltham, MA, USA). Membranes that were probed with more than one antibody were stripped before re-probing.

Intestinal permeability

Fluorescein Dextran (Molecular weight 3 kDa, diluted in HBSS) was gavaged (50 mg/g mouse). Four hours later, mouse blood samples were collected for fluorescence intensity measurement, as previously reported [21].

Immunofluorescence

Colonic tissues were freshly isolated and embedded in paraffin wax after fixation with 10% neutral buffered formalin. Immunofluorescence was performed on paraffin-embedded sections (4 μm), after preparation of the slides as described previously [22] followed by incubation for 1 hour in blocking solution (2% bovine serum albumin, 1% goat serum in HBSS) to reduce nonspecific background, as we previously reported [23]. The tissue samples were incubated overnight with primary antibodies at 4°C. The anti-Claudin-10 antibody was used. Slides were washed 3 times for 5 minutes each at room temperature in wash buffer. Samples were then incubated with secondary antibodies (goat anti-rabbit, Alexa Fluor 488, Molecular Probes, CA; 1:200) for 1 hour at room temperature. Tissues were mounted with SlowFade Antifade Kit (Life technologies, s2828, Grand Island, NY, USA), followed by a coverslip, and the edges were sealed to prevent drying. Specimens were examined with a Zeiss laser scanning microscope LSM 710 (Carl Zeiss Inc., Oberkochen, Germany).

Immunohistochemistry (IHC)

After preparation of the slides, antigen retrieval was achieved by incubating the slides for 15 min in hot preheated sodium citrate (pH 6.0) buffer and 30 min of cooling at room temperature. Endogenous peroxidases were quenched by incubating the slides in 3% hydrogen peroxide for 10 min, followed by three rinses with HBSS, and incubation for 1 hour in 3% BSA + 1% goat serum in HBSS to reduce nonspecific background. Primary antibodies VDR (1:300) were applied for overnight in a cold room. The secondary antibody (1:100, Jackson ImmunoResearch Laboratories, Cat.No.115-065-174, West Grove, PA, USA). The slides were incubated with vectastain ABC reagent (Vector Laboratories, Cat.No. PK-6100, Burlingame, CA 94010, USA) for 1 hour. After washing with HBSS, color development was achieved by applying a peroxidase substrate kit (Vector Laboratories, Cat.No. SK-4800, Burlingame, CA, USA). The duration of peroxidase substrate incubation was determined through pilot experiments and was then held constant for all of the slides. After washing in distilled water, the sections were counterstained with haematoxylin (Leica, Cat.No.3801570, Wetzlar, Germany), dehydrated through ethanol and xylene, and cover-slipped using a permount (Fisher Scientific, Cat.No. SP15-100, Waltham, MA, USA).

Fluorescence In Situ Hybridization

FISH was performed using antisense single-stranded DNA probes targeting the bacterial 16S ribosomal RNA [24]. The EUB338 (5'-GCTGCCTCCCGTAGGAGT-3') conjugated to Alexa Fluor488 probe was used for universal bacteria [25]. FISH was performed on paraffin sections of mucosal biopsies fixed with Carnoy's fixative or with 10% formalin solution. Before performing FISH assay, 5 μm tissue sections were baked overnight at 55°C. Tissue sections were deparaffinized in xylene, dehydrated with 100% ethanol, air dried, incubated in 0.2 mol/L HCl for 20 minutes, and heated in 1 mmol/L sodium thiocyanate at 80°C for 10 minutes. Samples were pepsin-digested (4% pepsin in 0.01 N HCl) for 20 minutes at 37°C), slides were washed in wash buffer (0.3 mol/L NaCl, 0.03 mol/L sodium citrate, pH 7, and 0.1% SDS), fixed in 10% buffered formalin for 15 minutes, washed and dried, and hybridized with the probes at 5 ng/μL concentration each for 5 minutes at 96°C in hybridization buffer (0.9 mol/L NaCl, 30% formamide, 20 mmol/L Tris-HCl, pH 7.4, and 0.01% SDS) and incubated at 37°C overnight. Slides were washed 4 times for 5 minutes each at 45°C in wash buffer. For visualization of the epithelial cell nuclei, the slides were counterstained with 4′, 6′-diamidino-2-phenylindole/antifade solution. Slides were examined with a Zeiss laser scanning microscope LSM 710 (Carl Zeiss, Inc). Fluorescence staining intensity was determined by using ImageJ software.

Alcian Blue /PAS staining

Alcian blue-PAS staining was performed on paraffin sections of colon tissue fixed with Carnoy's fixative. Before performing Alcian blue-PAS assay, 5 μm colon tissue sections were baked overnight at 55°C. Colon tissue sections were deparaffinized in xylene, dehydrated with 100% ethanol. The air-dry slides were stained with Alcian blue solution (1 g of Alcian blue, pH 2.5, 3 mL/L of acetic acid, and 97 mL of distilled water) for 30 min for goblet cells. This was followed by rinsing in tap water for 10 min, oxidizing in periodic acid (5 g/L) for 5 min, rinsing in tap water for 10 min, and staining in Schiff's reagent as a counter stain (Electron Microscopy Sciences, Cat. NO. 26853-01, Hatfield, PA, USA) for 10 min. After washing in distilled water for 10 minutes, dehydrated through ethanol and xylene, and cover-slipped using a permount (Fisher Scientific, Cat.No. SP15-100, Waltham, MA, USA).

Goblet cell- number-

Alcian blue-PAS-stained slides were used for counting goblet cells in the colon. Acidic (blue), neutral (pink), and mixed (purple) goblet cells were counted in each crypt. Goblet cell number was calculated by counting the average number of goblet cells in 3 crypts as one point. Three points were randomly selected for each mouse. Mean values for the number of goblet cells were calculated and analyzed using Welch's *t* test.

Multiplex ELISA assay

Mouse blood samples were collected by cardiac puncture and placed in tubes containing EDTA (10 mg/mL). Mouse cytokines were measured using a Cytokine & Chemokine Convenience 26-Plex Mouse ProcartaPlex™ Panel 1 (Invitrogen, EPXR260-26088-90, Carlsbad, CA, USA) according to the manufacturer's instructions. Briefly, beads of defined spectral properties were conjugated to protein-specific capture antibodies and added along with samples (including standards of known protein concentration, control samples, and test samples) into the wells of a filter-bottom microplate, where proteins bound to the capture antibodies over the course of a 2-hour incubation. After washing the beads, protein-specific biotinylated detector antibodies were added and incubated with the beads for 1 hour. After removal of excess biotinylated detector antibodies, the streptavidin-conjugated fluorescent protein R-phycoerythrin was added and allowed to incubate for 30 minutes. After washing to remove unbound streptavidin–R-phycoerythrin, the beads were analyzed with the Luminex detection system (Bio-rad, Bio-Plex 200 Systems, Hercules, CA).

Statistical analysis

All data were expressed as the mean ± SD. All statistical tests were 2-sided. All p-values < 0.05 were considered statistically significant. After the Shapiro-Wilk test confirmed that the data are normally distributed, the differences between samples were analyzed using unpaired Student's t-test for two groups and one-way ANOVA for more than two groups as appropriate, respectively. The p-values in ANOVA analysis were adjusted using the Tukey method to ensure accurate results. Pearson correlation analyses and scatter plots were conducted for staining intensity changes between VDR protein and Claudin-5, using SAS version 9.4 (SAS Institute, Inc., Cary, NC, USA) and R software (R Core Team (2021), R Foundation for Statistical Computing, Vienna, Austria). Other statistical analyses were performed using GraphPad Prism 6 (GraphPad, Inc., San Diego, CA., USA).

Results

Enhanced tumor-invading bacteria, reduced VDR, and decreased Claudin-10 in tumor samples from human CRC

In the human tumor samples, we identified enhanced bacteria by fluorescent in situ hybridization (**Fig. 1A**). We speculated that enhanced bacteria in tumors were associated with the status of VDR. We then tested intestinal VDR by IHC staining in normal colon controls and patients with colon cancer. Compared with the normal intestine, the intestine of patients had significantly lower VDR expression (n=10; Welch's *t* test) (**Fig. 1B**). At the mRNA level, we found reduced VDR expression in patients with colon cancer (GEO database GSE21510, Normal, n=44; colon cancer, n=104) (**Fig. 1E**). We believe the bacterial translocation to the tumors is related to the disrupted intestinal barrier functions through tight junctions (TJs). By IF staining, we showed the reduced TJ protein Claudin-10 and -5 in patients' samples, compared to the normal colon (**Fig. 1C and 1D**). Compared with normal intestines, colon cancer patients' intestines had significantly

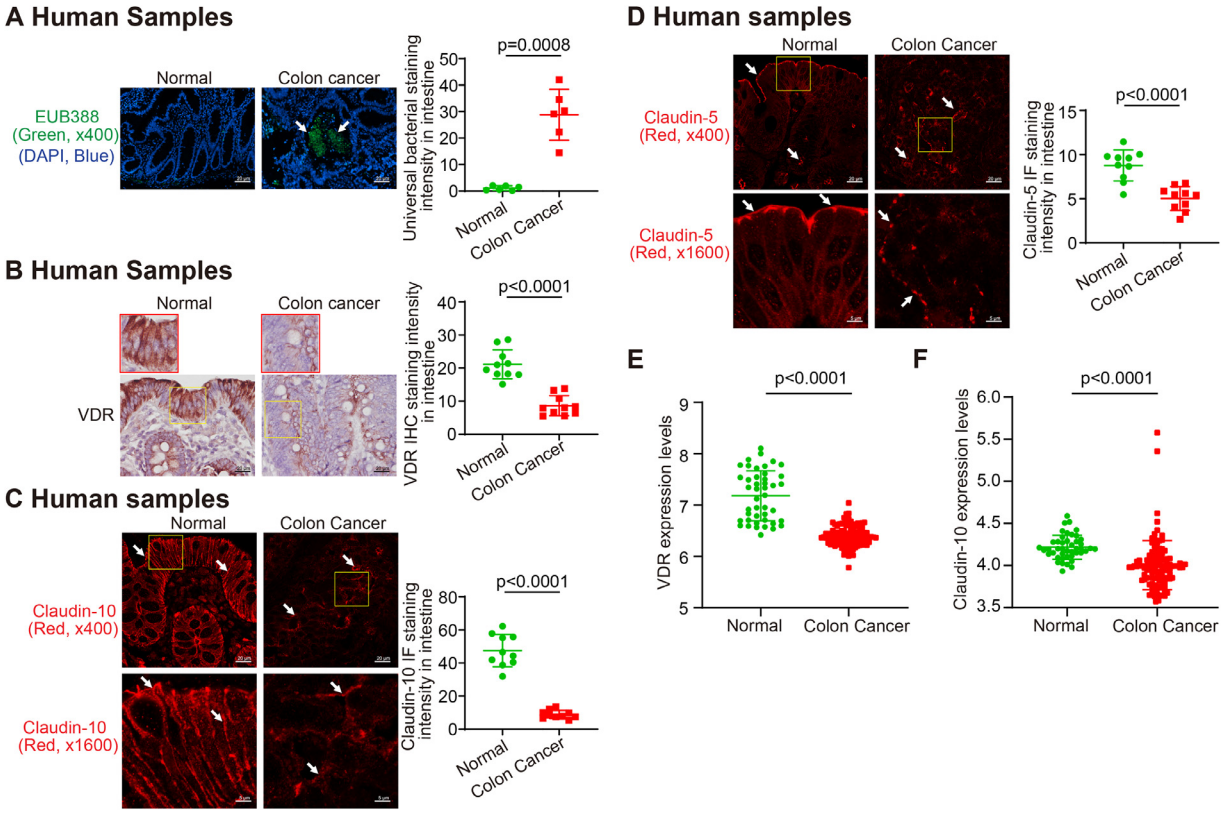

Fig. 1. Enhanced bacterial translocation, reduced VDR, and decreased Claudin-10 expression in CRC patients. (A) Bacteria in tumors from CRC patient by Fluorescence in situ hybridization [39]. (Images are representative of experiments in triplicate; normal, n = 6; colon cancer, n = 6; Welch's *t* test). **(B)** Significantly lowered VDR expression in the colon of CRC patients, compared with the normal intestines (Images are representative of three experiments; normal, n = 10; colon cancer, n = 10; Welch's *t* test). **(C)** Significantly reduced Claudin-10 in the colon of CRC patients, compared with the normal intestines. (Images are representative of experiments in triplicate; normal, n = 10; colon cancer, n = 10; Welch's *t* test). **(D)** Significantly reduced Claudin-5 in the colon of CRC patients, compared with the normal intestines. (Images are representative of three experiments; normal, n = 10; colon cancer, n = 10; Welch's *t* test). **(E)** Reduced VDR expression in patients with CRC (GEO database GSE21510, data were expressed as mean ± SD; normal, n = 44; colon cancer, n = 104; Welch's *t* test). **(F)** Reduced Claudin-10 expression in patients with CRC (GEO database GSE21510, data were expressed as mean ± SD; normal, n = 44; colon cancer, n = 104; Welch's *t* test). All *p* values are shown in the figure.

lower Claudin-10 mRNA expression (GEO database GSE21510, data were expressed as mean ± SD; Normal, n=44; colon cancer, n=104) colon (**Fig. 1F**). These data indicate the reduced VDR in the colon of CRC patients is associated with the reduced intestinal tight junctions for barrier and enhanced bacterial translocation to tumors.

Intestinal VDR-specific knockout led to reduced mucus thickness in colonic tumors

To investigate the mechanism of host factor regulation of microbiome and intestinal barrier function, we then examined the animal models with intestinal VDR deletion in the intestinal epithelial cells ($VDR^{\Delta IEC}$) or myeloid cells ($VDR^{\Delta Lyz}$) [26–28]. The $VDR^{\Delta IEC}$ mice were known to be susceptible to the chemical-induced tumorigenesis in the colon, based on our recent reports [9,26]. Here, we found that mucus thickness declined in the colon of $VDR^{\Delta IEC}$ mice, compared to the VDR^{Loxp} mice, without any treatment (**Fig. 2A**). In addition to the narrowed mucus layer, there was dislocation of intestinal microbiota from the lumen to the gut epitheliums and tumor tissue. However, in the VDR overexpressed mice and their loxp controls, we did not find the changes in the mucus thickness or bacterial penetrations (**Fig. 2B**). We further examine the mucus layer by Alcian Blue/PAS staining in the colon of VDR^{Loxp} and $VDR^{\Delta IEC}$ mice. The narrowed mucus layer was significant in the colon of $VDR^{\Delta IEC}$ mice (**Fig. 2C**). Goblet cells were significantly reduced on the the colon of $VDR^{\Delta IEC}$ mice, compaed to the VDR^{Loxp} mice (**Fig. 2D**). Bacteria were increased in the tumor tissue of $VDR^{\Delta IEC}$ mice, compared to the tumor tissue of VDR^{Loxp} mice (**Fig. 2E**). Moreover, TJ Claudin-10 distribution in the colonic epithelial cells was decreased in $VDR^{\Delta IEC}$ mice compared to VDR^{loxp} mice at basal level. Claudin-10 was further decreased in tumors of $VDR^{\Delta IEC}$ mice, compared to those of VDR^{Loxp} mice by immunofluorescence staining (**Fig. 2F**). The reduced Claudin-10 protein in $VDR^{\Delta IEC}$ mice was further confirmed by Western blots (**Fig. 2G**), whereas TJ Claudin-3, 4, and 7 did not change with the VDR status. Please note that the level of colonic Claudin-10 protein was significantly reduced in the $VDR^{\Delta IEC}$ mice compared to VDR^{loxp} mice without any treatment. It is known that tumorigenesis is related to the microbial dysbiosis, narrowed mucus layer, and damaged barrier functions. These data suggest that the host regulation of barrier dysfunction was preexisting pre-cancer and got worse in the tumor development.

Mice with myeloid VDR deletion developed more and larger tumors, compared to the VDR^{Loxp} mice

We then studied the $VDR^{\Delta Lyz}$ mice with myeloid VDR deletion to understand the role of immunity in the interplays among the host factor, microbial dysbiosis, and barrier functions. $VDR^{\Delta Lyz}$ mice and their VDR^{Loxp} controls were treated with the AOM/DSS to induce colon cancer (**Fig. 3A**).

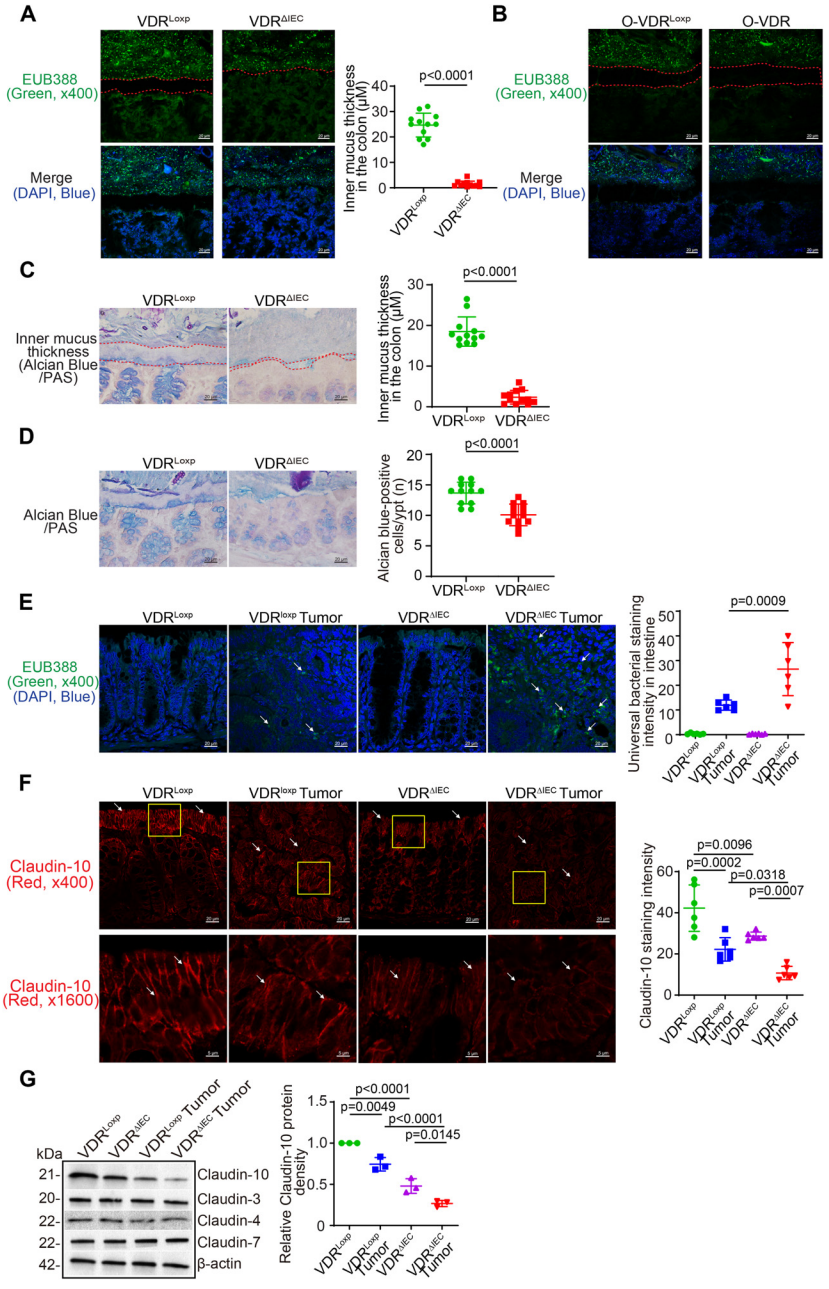

Fig. 2. Intestinal epithelial VDR-specific knockout reduced mucus thickness, enhanced bacterial penetration, and reduced Claudin-10 expression in the VDR$^{\Delta IEC}$ mice. **(A)** Colonic mucus thickness declined in the VDR$^{\Delta IEC}$ mice, compared to the VDR^{Loxp} mice. Representative images of FISH staining of the colon of VDR^{Loxp} and VDR$^{\Delta IEC}$ mice, using the universal bacterial DNA probe EUB338-Alexa Fluor 488 [40], and nuclear staining DAPI (blue). The space between apical membranes of the epithelial cells and gut microbiome was indicated by dashed red lines. Images are from a single experiment and are representative of 4 mice per group. Three points were randomly selected for each mouse (data are expressed as mean ± SD. n = 12, Welch's *t* test). **(B)** Colonic mucus thickness was not changed in the O-VDR mice, compared to O-VDR^{Loxp} mice. Images are from a single experiment and are representative of 4 mice per group. **(C)** Mucus thickness declined in the colon of VDR$^{\Delta IEC}$ mice compared to VDR^{Loxp} mice. Representative images of Alcian Blue/PAS staining of the colon of VDR^{Loxp} and VDR$^{\Delta IEC}$ mice. The space between apical membranes of the epithelial cells and gut microbiome was indicated by dashed red lines. Images are from a single experiment and are representative of 4 mice per group. Three points were randomly selected for each mouse (data are expressed as mean ± SD. n = 12, Welch's *t* test). **(D)** Reduced Goblet cells in the colon of VDR$^{\Delta IEC}$ mice, compared to VDR^{Loxp} mice. Images are from a single experiment and are representative of 4 mice per group. Three points were randomly selected for each mouse (data are expressed as mean ± SD. n = 12, Welch's *t* test). **(E)** Enhanced bacteria in the tumors of the VDR$^{\Delta IEC}$ mice, as indicated in FISH staining. Images are from a single experiment and are representative of 6 mice per group (data are expressed as mean ± SD. n= 6, one-way ANOVA test) [41]. Claudin-10 was decreased in VDR$^{\Delta IEC}$ mice, compared to the VDR^{Loxp} mice at the basal level. Claudin-10 was further decreased in tumors of the VDR$^{\Delta IEC}$ mice by immunofluorescence staining. Images are from a single experiment and are representative of 6 mice per group (data are expressed as mean ± SD. n=6, one-way ANOVA test). **(G)** Claudin-10 was decreased in VDR$^{\Delta IEC}$ mice compared to VDR^{loxp} mice at the basal level and also in tumors by Western blots. (data are expressed as mean ± SD. n=3, one-way ANOVA test). All *p* values are shown in the figure.

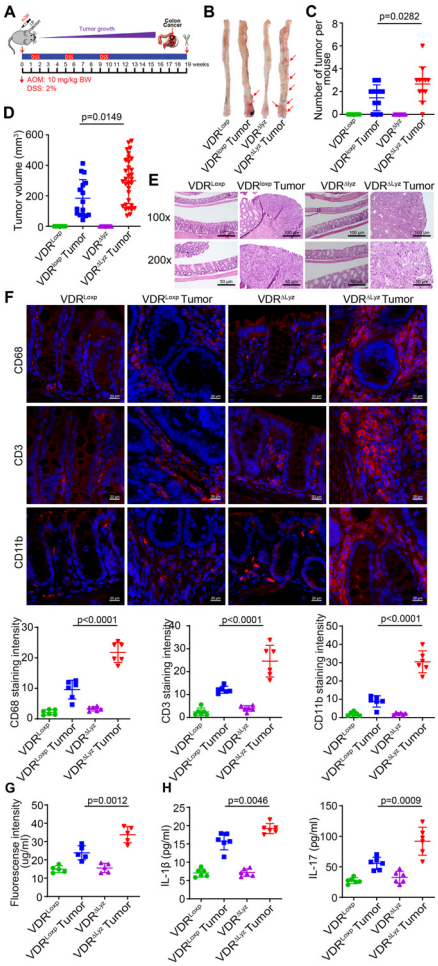

Fig. 3. VDR$^{\Delta Lyz}$ mice with Myeloid VDR deletion developed more and larger tumors, compared with the VDR^{loxp} mice. (A) A schematic overview of the AOM/DSS-induced colon cancer model. AOM (10 mg/kg) was injected on day 0. Starting at Day 7, 2% DSS solution was administered to mice in drinking water with a duration of 7 days. Then, the mice were given DSS-free drinking water for 3 weeks. After that, an additional two cycles of DSS drinking water were administered prior to scarification at Week 19. **(B)** Colonic tumors *in situ.* Representative colons from different groups. Tumors were indicated with red arrows. **(C)** Tumor numbers in AOM-DSS induced colon cancer model: VDR^{Loxp} and VDR$^{\Delta Lyz}$ mice (data are expressed as mean ± SD. n = 8, 11, 10, and 12 for the VDR^{Loxp} control, VDR^{Loxp} tumor, VDR$^{\Delta Lyz}$ control, and VDR$^{\Delta Lyz}$ tumor groups, one-way ANOVA test). **(D)** The tumor volume in AOM-DSS induced colon cancer model: VDR$^{+/+}$ and VDR$^{-/-}$ mice (data are expressed as mean ± SD. n = 8, 11, 10, and 12 for the VDR^{Loxp} control, VDR^{Loxp} tumor, VDR$^{\Delta Lyz}$ control, and VDR$^{\Delta Lyz}$ tumor groups, respectively; one-way ANOVA test). **(E)** Representative H&E staining of "Swiss rolls" of representative colons from the indicated groups. Images are from a single experiment and are representative of 6 mice per group. **(F)** Levels of CD68, CD3, and CD11b were increased significantly in the tumor tissues of VDR$^{\Delta Lyz}$ mice, compared to the tumor tissues of VDR^{Loxp} mice by IF staining. Images are from a single experiment and are representative of 6 mice per group (data are expressed as mean ± SD. n = 6, one-way ANOVA test). All *p* values are shown in the figure. **(G)**Intestine permeability increased in the VDR$^{\Delta Lyz}$ mice with tumors. Experiments were assayed in triplicates (data are expressed as mean ± SD; n = 5, one-way ANOVA test). **(H)** Serum cytokines IL-1β and IL-17 were significantly increased in the AOM-DSS-treated VDR$^{\Delta Lyz}$ mice. Experiments were assayed in triplicates (data are expressed as mean ± SD. n= 6, one-way ANOVA test). All *p* values are shown in the figure.

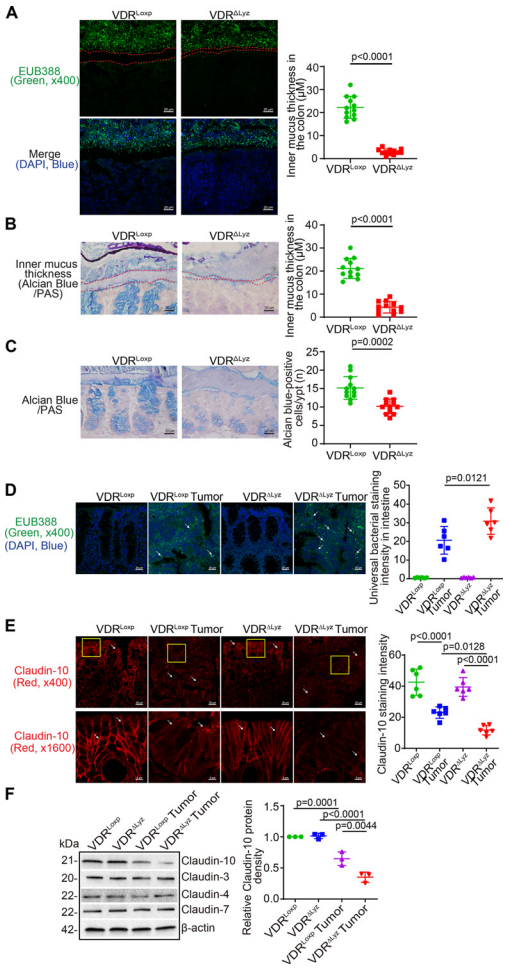

Fig. 4. Myeloid cells VDR-specific knockout led to reduced mucus thickness, bacterial dislocation, and reduced Claudin-10 expression tumor tissues of VDR$^{\Delta Lyz}$ mice. (A) Mucus thickness decline in the colon of the VDR$^{\Delta Lyz}$ mice in FISH staining. Images are from a single experiment and are representative of 4 mice per group. Three points were randomly selected for each mouse. (Data are expressed as mean ± SD. n = 12, Welch's *t* test). **(B)** Mucus thickness decline in the VDR$^{\Delta Lyz}$ mice colon compared to VDR^{Loxp} mice. Representative images of Alcian Blue/PAS staining of the colon of VDR^{Loxp} and VDR$^{\Delta Lyz}$ mice. The space between apical membranes of the epithelial cells and gut microbiome is indicated by a dashed red line. Images are from a single experiment and are representative of 4 mice per group. Three points were randomly selected for each mouse (data are expressed as mean ± SD. n = 12, Welch's *t* test). **(C)** Goblet cells number decreased in the VDR$^{\Delta Lyz}$ mice colon compared to VDR^{Loxp} mice. Images are from a single experiment and are representative of 4 mice per group. Three points were randomly selected for each mouse (data are expressed as mean ± SD. n = 12, Welch's *t* test). (**D**) Bacteria were increased in the tumors of VDR$^{\Delta Lyz}$ mice as indicated. Images are from a single experiment and are representative of 6 mice per group (data are expressed as mean ± SD. n = 6, one-way ANOVA test). (**E**) Claudin-10 was decreased in the tumors of VDR$^{\Delta Lyz}$ mice, compared to VDR^{Loxp} mice by immunofluorescence staining. Images are from a single experiment and are representative of 6 mice per group (data are expressed as mean ± SD. n = 6, one-way ANOVA test) [41]. Claudin-10 was decreased in tumor tissue of VDR$^{\Delta Lyz}$ mice by Western blots (data are expressed as mean ± SD. n = 3, one-way ANOVA test). Claudin-3, Claudin-4 and Claudin-7 were unchanged in the colon of VDR$^{\Delta Lyz}$ mice compared to VDR^{Loxp} mice treated with AOM/DSS. All *p* values are shown in the figure.

Representative colons from different groups and colonic tumors *in situ* were shown *in* **Fig. 3B**. Tumor numbers and volumes in the $VDR^{\Delta Lyz}$ mice were significantly greater than those in the VDR^{Loxp}-AOM/DSS group (**Fig. 3C and 3D**). Representative H&E staining of "Swiss rolls" of representative colons from the indicated groups (**Fig. 3E**). Levels of CD68, CD3, and CD11b for immune cells (monocyte/macrophages, granulocytes, and natural killer cells) were increased significantly in the tumor tissues of $VDR^{\Delta Lyz}$ mice, compared to those in VDR^{Loxp} mice **(Fig. 3F).** Permeability of the $VDR^{\Delta Lyz}$ mice was significantly increased measured by fluorescence intensity in serum **(Fig. 3G).** Serum cytokines, such as IL-1β and IL-17, were also significantly increased in the AOM-DSS-treated $VDR^{\Delta Lyz}$ mice **(Fig. 3H),** suggesting increased inflammation in the mice.

Myeloid cells VDR-specific knockout induced mucus thickness decline, bacterial translocation, and reduced Claudin-10 in the colon

As expected, colonic mucus thickness declined in the $VDR^{\Delta Lyz}$ mice colon, compared to VDR^{Loxp} mice **(Fig. 4A)**. The status of mucus layer was further confirmed by Alcian Blue/PAS staining. The narrowed mucus layer was significant in the colon of $VDR^{\Delta Lyz}$ mice (**Fig. 4B**). Goblet cells were significantly reduced on the the colon of $VDR^{\Delta Lyz}$ mice, compared to the VDR^{Loxp} mice (**Fig. 4C**). Bacteria were increased in the tumors of $VDR^{\Delta Lyz}$ mice, compared to those of VDR^{Loxp} mice **(Fig. 4D)**. TJ Claudin-10 was significantly decreased in $VDR^{\Delta Lyz}$ mice with tumors **(Fig. 4E).** The reduced Claudin-10 at the protein level in $VDR^{\Delta IEC}$ mice was further confirmed by Western blots, whereas TJ Claudins 3, 4, and 7 did not change with the VDR status in the myeloid cells (**Fig. 4F**).

Reduced mucus thickness, enhanced bacteria, and decreased Claudin-10 in tumors spontaneously developed in the $APC^{15\Delta CEC}$ mice.

To study the host factor regulation of altered mucus layer and bacterial translocation to tumors we then use another colon cancer model: $APC^{15\Delta CEC}$ CRC model [29,30]. Colonic APC knockout ($APC^{15\Delta CEC}$) mice were generated by breeding APC^{15Loxp} mice and CDX2P-NLS Cre mice. $APC^{15\Delta CEC}$ mice spontaneously developed colonic tumors at >21-week old at the UIC animal facility. We investigated the changes of barrier and microbiome in the spontaneous tumor formation process in the $APC^{15\Delta CEC}$ mice. Colonic mucus thickness was reduced in the $APC1^{15\Delta CEC}$ mice, compared to that in the APC^{15Loxp} mice **(Fig. 5A).** Bacteria were signifcantly increased in tumors of $APC1^{15\Delta CEC}$ mice **(Fig. 5B).** Claudin-10 was decreased in $APC^{15\Delta CEC}$ mice, compared to APC^{15Loxp} mice by IF (**Fig. 5C**) and Western blots (**Fig. 5D**). However, Claudins- 3, 4 and 7 did not change in the colon of $APC^{15\Delta CEC}$ mice compared to APC^{15Loxp} mice (**Fig. 5D**). These data suggest that the genetic factor of APC mutation in the colon could lead to altered microbiome distribution and disrupted barriers.

Discussion

In the current study, we reported that a host factor, conditional VDR deficiency or colonic APC mutation, led to the reduced thickness of mucus layer and enhanced penetration of microbiota into the epithelial cells, thus enhancing colonic tumorigenesis. In the healthy colon, the microbiota, mucus layer, epithelial tight junctions, and local immune cells keep the host from inflammation and cancer. However, the microbial dysbiosis, narrowed mucus layer, and damaged barrier functions by modifying regulators enhance the tumorigenesis. Moreover, these dysfunctional changes further induce the dislocation of microbiota from the lumen to the epitheliums and tumor tissue. Previous studies have demonstrated that conditional VDR deletion in intestinal epithelial cells led to dysbiosis [28,31,32]. Here, our data from human samples and various cancer models provided solid evidences on the host factor regulation of local dysbiosis, bacterial penetration to the epithelial cells, and dysfunction on barriers in the colon pre-cancer or in the development of cancer.

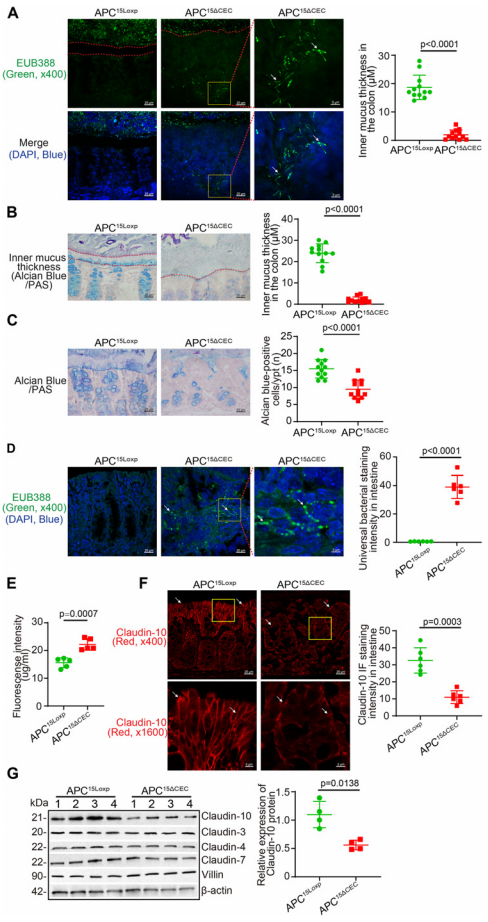

Fig. 5. Reduced mucus thickness and decreased Claudin-10 expression in the colon of $APC^{15\Delta CEC}$ mice. (A) Mucus thickness in the colon were reduced in the $APC^{15\Delta CEC}$ mice, compared to APC^{15Loxp} mice. Bacteria were enhanced in the tumors of $APC^{15\Delta CEC}$ mice. Images are from a single experiment and are representative of 4 mice per group. Three points were randomly selected for measurement per mouse (data are expressed as mean ± SD. n = 12, Welch's *t* test). **(B)** Mucus thickness decline in the $APC^{15\Delta CEC}$ mice colon by Alcian Blue/PAS staining. Representative images of Alcian Blue/PAS staining of the colon of APC^{15Loxp} and $APC^{15\Delta CEC}$ mice. The apical membranes of the epithelial cells and gut microbiome are indicated by dashed red lines. Images are from a single experiment and are representative of 4 mice per group. Three points were randomly selected for each mouse (data are expressed as mean ± SD. n = 12, Welch's *t* test). **(C)** The numbers of goblet cells were reduced in the $APC^{15\Delta CEC}$ mice colon compared to APC^{15Loxp} mice. Images are from a single experiment and are representative of 4 mice per group. Three points were randomly selected for measurement per mouse (data are expressed as mean ± SD. n = 12, Welch's *t* test). All *p* values are shown in the figure. (**D**) Bacteria were increased in 10% formalin-fixed tumor tissues of $APC^{15\Delta CEC}$ mice. Images are from a single experiment and are representative of 6 mice per group (data are expressed as mean ± SD. n = 6, one-way ANOVA test). **(E)** Intestine permeability increased in the $APC^{15\Delta CEC}$ mice compared to APC^{15Loxp} mice (data are expressed as mean ± SD. n = 5, Welch's *t* test). (**F**) Claudin-10 was decreased in $APC^{15\Delta CEC}$ mice compared to APC^{15Loxp} mice. Images are from a single experiment and are representative of 6 mice per group (data are expressed as mean ± SD. n = 6, one-way ANOVA test). **(G)** Claudin-10 was decreased in in $APC^{15\Delta CEC}$ mice, compared to the APC^{15Loxp} mice by Western blots (data are expressed as mean ± SD. n = 4, Welch's *t* test). Claudin-3, Claudin-4 and Claudin-7 were unchanged in the colon of $APC^{15\Delta CEC}$ mice compared to the APC^{15Loxp} mice. All *p* values are shown in the figure.

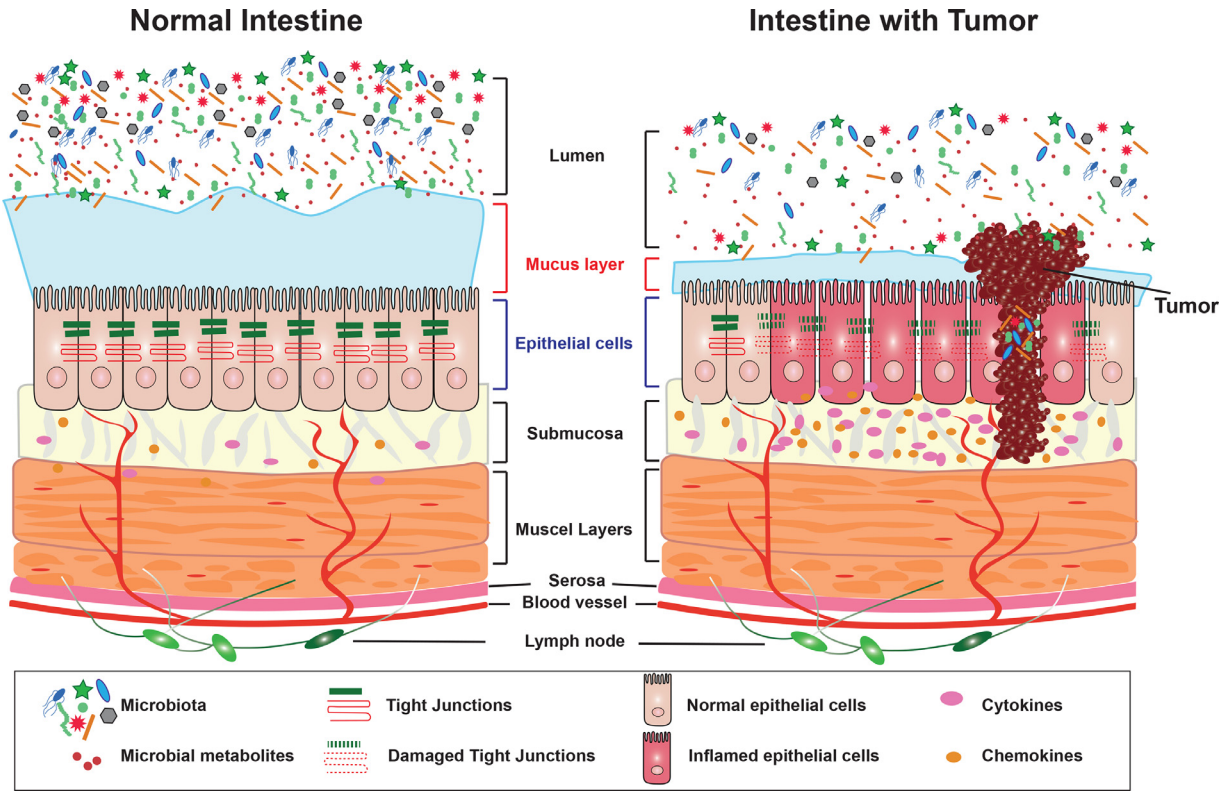

Fig. 6. The working model for the host factor in regulating protective microbiota, mucus layer, and epithelial barriers. In the healthy intestine, the balanced microbiota, strong mucus layer and protective epithelial barriers keep the intestine from inflammation and tumorigenesis. However, in the susceptible host (e.g., VDR deficiency, APC mutation), there is preexisting barrier dysfunction and dysbiosis. The tumor development worsens the microbial dysbiosis, narrows mucus layer, and damages barrier functions by modifying tight junctions (TJs). Moreover, these dysfunctional changes could further induce the dislocation of microbiota from the lumen to the intestinal epithelium and tumors.

TJ protein Claudins have a big family with at least 27 members in mouse and human [33]. A previous study showed expression profiles of *some CLDN* genes and prognostic value in CRC samples classified by their molecular subtypes. It suggested that CRC heterogeneity must be taken into account when assessing *CLDN* potential value as prognostic markers or therapeutic targets [34]. We explored the human datasets and reported that the mRNA expression of Claudin -1, -2, -12, -19 were increased in colon cancer patients; the mRNA expression of Claudin -5, -8, -15, -17, -20, -23 were decreased in patients with colon cancer. Claudin -3, -4, -6, -7, -9, -10, -11, -14, -16, -18 did not show distinct changes at the mRNA level between patients with colon cancer and normal controls. However, these observations are only at the mRNA levels. The biological functions of junction proteins rely on their protein distributions and interactions with other junctional proteins. The level of mRNA could not completely reflect the biological and pathological functions of junction proteins in the development of cancer. Currently, there are limited cellular studies on the individual Claudin protein and its alteration by the upstream regulator from the host. Our data on the Claudin-10 distribution and protein level in the human CRC tumors and chemical-induced and genetic colon cancer models start to fill the gap in the field.

VDR was a transcriptional factor regulating the genes of several TJ Claudins [35,36]. The positively correlated status of VDR and Claudins (e.g., Claudin-5, and 15) contributes to the altered intestinal permeability in chronic inflammation and tumorigenesis [21,26,37]. We have demonstrated that conditional VDR deletion in a tissue specific manner led to dysbiosis [27,28,31,32]. In the intestinal epithelial VDR knockout $VDR^{\Delta IEC}$ mice and $VDR^{\Delta lyz}$ mice, dysbiosis and inflammatory cytokines in the VDR deficient context altered TJs and manipulated the barrier functions. Our current studies showed narrowed mucus layer and bacterial translocation, which weakens the multiple layers of the intestinal barriers in absence of VDR. Moreover, the narrow mucus layer and bacterial translocation in the $APC^{15\Delta CEC}$ mice validate the role of host factor in a genetic cancer model. These studies provide strong rationale and an additional avenue to restore microbiome and barrier functions for risk assessment and prevention of CRC in the future [38].

In the current study, we have demonstrated the importance of myeloid VDR in barrier function and protecting the host against tumorigenesis. Without any treatment, $VDR^{\Delta Lyz}$ mice already showed less mucus layer and bacterial penetration to the epithelial cells, compared to the VDR^{Loxp} mice. Tumor numbers and volumes were significantly greater in the AOM/DSS treated $VDR^{\Delta Lyz}$ mice than those in the VDR^{Loxp} with the AOM/DSS. VDR deficiency in the immune cells leads to less epithelial Claudin 10, more infiltration, increased inflammation, suggesting the cross talks between the local immune cells and epithelial cells in the colon. $VDR^{\Delta Lyz}$ mice are known with reduced beneficial bacterial profile and altered functions of metabolites based on our previous studies [27,28]. All together, these results provide us with insights into the innate immunity in the interplays among the host factor, microbial dysbiosis, and intestinal barrier functions. It is known that balanced microbiota, strong mucus layer, epithelial barriers, and local immunity together protect the intestine against inflammation and cancer. Further studies are needed to understand of the mechanisms and impacts of the dynamic interactions of microbiota, immune cells, and epithelial cells in health and cancer.

In summary, our studies from human samples and various colon cancer models have provided evidence on the host factor regulation of dysbiosis and

barrier dysfunction in the pre-cancer or in the development of cancer. For the long-run, insights into the host - microbiome interactions and barriers could be potentially applied to risk assessment, early detection, and prevention of colon cancer and other cancers, as well.

Author contributions

YZ: acquisition, analysis, and interpretation of data; drafting the manuscript; and statistical analysis. JZ: assistance with animal models, Western blots, and manuscript and figure drafting. YX: statistical analysis, and manuscript drafting. JS: study concept and design, analysis and interpretation of data, writing the manuscript for important intellectual content, obtained funding, and study supervision.

Acknowledgments

We would like to thank Jason S. Xia for proofreading.

References

[1] Song M, Chan AT, Sun J. Influence of the gut microbiome, diet, and environment on risk of colorectal cancer. *Gastroenterology* 2020;**158**:322–40.

[2] Sun J, Kato I. Gut microbiota, inflammation and colorectal cancer. *Genes Dis* 2016;**3**:130–43.

[3] Sun J. Impact of bacterial infection and intestinal microbiome on colorectal cancer development. *Chin Med J* 2021 **In press**.

[4] Fletcher R, Wang YJ, Schoen RE, Finn OJ, Yu J, Zhang L. Colorectal cancer prevention: Immune modulation taking the stage. *Biochim Biophys Acta Rev Cancer* 2018;**1869**:138–48.

[5] Yang J, Wei H, Zhou Y, Szeto CH, Li C, Lin Y, Coker OO, Lau HCH, Chan AWH, Sung JJY, et al. High-fat diet promotes colorectal tumorigenesis through modulating gut microbiota and metabolites. *Gastroenterology* 2022;**162**:135–49 e132.

[6] Kwong TNY, Wang X, Nakatsu G, Chow TC, Tipoe T, Dai RZW, Tsoi KKK, Wong MCS, Tse G, Chan MTV, et al. Association between bacteremia from specific microbes and subsequent diagnosis of colorectal cancer. *Gastroenterology* 2018;**155**:383–90 e388.

[7] Horas K, Zheng Y, Fong-Yee C, Macfarlane E, Manibo J, Chen YZ, Qiao J, Gao MX, Haydar N, McDonald MM, et al. Loss of the Vitamin D receptor in human breast cancer cells promotes epithelial to mesenchymal cell transition and skeletal colonization. *J Bone Miner Res* 2019;**34**:1721–32.

[8] Zeissig S, Burgel N, Gunzel D, Richter J, Mankertz J, Wahnschaffe U, Kroesen AJ, Zeitz M, Fromm M, Schulzke JD. Changes in expression and distribution of claudin 2, 5 and 8 lead to discontinuous tight junctions and barrier dysfunction in active Crohn's disease. *Gut* 2007;**56**:61–72.

[9] Zhang YG, Lu R, Wu S, Chatterjee I, Zhou D, Xia Y, Sun J. Vitamin D receptor protects against dysbiosis and tumorigenesis via the JAK/STAT pathway in intestine. *Cell Mol Gastroenterol Hepatol* 2020;**10**:729–46.

[10] Dove WF, Cormier RT, Gould KA, Halberg RB, Merritt AJ, Newton MA, Shoemaker AR. The intestinal epithelium and its neoplasms: genetic, cellular and tissue interactions. *Philos Trans R Soc Lond B Biol Sci* 1998;**353**:915–23.

[11] Barrett JC, Hansoul S, Nicolae DL, Cho JH, Duerr RH, Rioux JD, Brant SR, Silverberg MS, Taylor KD, Barmada MM, et al. Genome-wide association defines more than 30 distinct susceptibility loci for Crohn's disease. *Nat Genet* 2008;**40**:955–62.

[12] Tsukamoto S, Ishikawa T, Iida S, Ishiguro M, Mogushi K, Mizushima H, Uetake H, Tanaka H, Sugihara K. Clinical significance of osteoprotegerin expression in human colorectal cancer. *Clin Cancer Res* 2011;**17**:2444–50.

[13] Van Cromphaut SJ, Dewerchin M, Hoenderop JG, Stockmans I, Van Herck E, Kato S, Bindels RJ, Collen D, Carmeliet P, Bouillon R, et al. Duodenal calcium absorption in vitamin D receptor-knockout mice: functional and molecular aspects. *Proc Natl Acad Sci U S A* 2001;**98**:13324–9.

[14] Y-g Zhang, R Lu, Xia Y, Zhou D, Petrof E, Claud EC, Sun J. Lack of vitamin D receptor leads to hyperfunction of claudin-2 in intestinal inflammatory responses. *Inflammatory Bowel Diseases* 2018;**25**:97–110.

[15] Zhang Y-G, Lu R, Wu S, Chatterjee I, Zhou D, Xia Y, Sun J (2020). Vitamin D receptor protects against dysbiosis and tumorigenesis via the JAK/STAT pathway in intestine *Biorxiv* **02**.

[16] Wu S, Zhang YG, Lu R, Xia Y, Zhou D, Petrof EO, Claud EC, Chen D, Chang EB, Carmeliet G, et al. Intestinal epithelial vitamin D receptor deletion leads to defective autophagy in colitis. *Gut* 2015;**64**:1082–94.

[17] Lu R, Zhang Y, Xia Y, Zhang J, Kaser A, Blumberg R, Sun J. Paneth cell alertness to pathogens maintained by vitamin D receptors. *Gastroenterology* 2020.

[18] Chatterjee I, Zhang Y, Zhang J, Lu R, Xia Y, Sun J. Overexpression of vitamin D receptor in intestinal epithelia protects against colitis via upregulating tight junction protein claudin 15. *J Crohn's Colitis* 05 March, 2021.

[19] Lu R, Wu S, Zhang YG, Xia Y, Liu X, Zheng Y, Chen H, Schaefer KL, Zhou Z, Bissonnette M, et al. Enteric bacterial protein AvrA promotes colonic tumorigenesis and activates colonic beta-catenin signaling pathway. *Oncogenesis* 2014;**3**:e105.

[20] Lu R, Wu S, Zhang YG, Xia Y, Zhou Z, Kato I, Dong H, Bissonnette M, Sun J. Salmonella protein AvrA activates the STAT3 signaling pathway in colon cancer. *Neoplasia* 2016;**18**:307–16.

[21] Zhang YG, Lu R, Xia Y, Zhou D, Petrof E, Claud EC, Sun J. Lack of Vitamin D receptor leads to hyperfunction of claudin-2 in intestinal inflammatory responses. *Inflamm Bowel Dis* 2019;**25**:97–110.

[22] Lu R, Wu S, Liu X, Xia Y, Zhang YG, Sun J. Chronic effects of a Salmonella type III secretion effector protein AvrA in vivo. *PLoS One* 2010;**5**: e10505.

[23] Zhang YG, Zhu X, Lu R, Messer JS, Xia Y, Chang EB, Sun J. Intestinal epithelial HMGB1 inhibits bacterial infection via STAT3 regulation of autophagy. *Autophagy* 2019.

[24] DeLong EF, Wickham GS, Pace NR. Phylogenetic stains: ribosomal RNA-based probes for the identification of single cells. *Science* 1989;**243**:1360–3.

[25] Tan SM, Yung PYM, Hutchinson PE, Xie C, Teo GH, Ismail MH, Drautz-Moses DI, Little PFR, Williams RBH, Cohen Y. Primer-free FISH probes from metagenomics/metatranscriptomics data permit the study of uncharacterised taxa in complex microbial communities. *NPJ Biofilms Microbiomes* 2019;**5**: 17.

[26] Zhang Y, Garrett S, Carroll RE, Xia Y, Sun J. Vitamin D receptor upregulates tight junction protein claudin-5 against colitis-associated tumorigenesis. *Mucosal Immunol* 2022.

[27] Chatterjee I, Lu R, Zhang Y, Zhang J, Dai Y, Xia Y, Sun J. Vitamin D receptor promotes healthy microbial metabolites and microbiome. *Sci Rep* 2020;**10**:7340.

[28] Zhang J, Zhang Y, Xia Y, Sun J. Imbalance of the intestinal virome and altered viral-bacterial interactions caused by a conditional deletion of the vitamin D receptor. *Gut Microbes* 2021;**13**:1957408.

[29] Robanus-Maandag EC, Koelink PJ, Breukel C, Salvatori DC, Jagmohan-Changur SC, Bosch CA, Verspaget HW, Devilee P, Fodde R, Smits R. A new conditional Apc-mutant mouse model for colorectal cancer. *Carcinogenesis* 2010;**31**:946–52.

[30] Flisikowska T, Merkl C, Landmann M, Eser S, Rezaei N, Cui X, Kurome M, Zakhartchenko V, Kessler B, Wieland H, et al. A porcine model of familial adenomatous polyposis. *Gastroenterology* 2012;**143** 1173-1175 e1177.

[31] Lu R, Zhang YG, Xia Y, Zhang J, Kaser A, Blumberg R, Sun J. Paneth cell alertness to pathogens maintained by vitamin D receptors. *Gastroenterology* 2021;**160**:1269–83.

[32] Wu S, Yoon S, Zhang YG, Lu R, Xia Y, Wan J, Petrof EO, Claud EC, Chen D, Sun J. Vitamin D receptor pathway is required for probiotic protection in colitis. *Am J Physiol Gastrointest Liver Physiol* 2015;**309**:G341–9.

[33] Mineta K, Yamamoto Y, Yamazaki Y, Tanaka H, Tada Y, Saito K, Tamura A, Igarashi M, Endo T, Takeuchi K, et al. Predicted expansion of the claudin multigene family. *FEBS Lett* 2011;**585**:606–12.

[34] Cherradi S, Martineau P, Gongora C, Del Rio M. Claudin gene expression

profiles and clinical value in colorectal tumors classified according to their molecular subtype. *Cancer Manag Res* 2019;**11**:1337–48.

[35] Yong-guo Zhang SW, Lu Rong, Zhou David, Wan Jiandi, Zhou Jingsong, Carmeliet Geert, Petrof Elaine, Claud Erika C, Sun Jun. Tight junction CLDN2 gene is a direct target of the vitamin D receptor. *Scientific Report* 2015 **in press**.

[36] Zhang YG, Wu S, Sun J. Vitamin D, Vitamin D receptor, and tissue barriers. *Tissue Barriers* 2013;**1**.

[37] Chatterjee I, Zhang Y, Zhang J, Lu R, Xia Y, Sun J. Overexpression of Vitamin D receptor in intestinal epithelia protects against colitis via upregulating tight junction protein Claudin 15. *J Crohns Colitis* 2021;**15**:1720–36.

[38] Sun J, Zhang YG. Vitamin D receptor influences intestinal barriers in health and disease. *Cells* 2022;**11**.

[39] Li XY, Boudjelal M, Xiao JH, Peng ZH, Asuru A, Kang S, Fisher GJ, Voorhees JJ. 1,25-Dihydroxyvitamin D3 increases nuclear vitamin D3 receptors by blocking ubiquitin/proteasome-mediated degradation in human skin. *Mol Endocrinol* 1999;**13**:1686–94.

[40] Hinoi T, Akyol A, Theisen BK, Ferguson DO, Greenson JK, Williams BO, Cho KR, Fearon ER. Mouse model of colonic adenoma-carcinoma progression based on somatic Apc inactivation. *Cancer Res* 2007;**67**:9721–30.

[41] Boivin GP, Washington K, Yang K, Ward JM, Pretlow TP, Russell R, Besselsen DG, Godfrey VL, Doetschman T, Dove WF, et al. Pathology of mouse models of intestinal cancer: consensus report and recommendations. *Gastroenterology* 2003;**124**:762–77.